ACS APPLIED MATERIALS & INTERFACES
Research Article
www.acsami.org

Structure and Electrical Properties of Al-Doped HfO_2 and ZrO_2 Films Grown via Atomic Layer Deposition on Mo Electrodes

Yeon Woo Yoo,[†] Woojin Jeon,[†] Woongkyu Lee,[†] Cheol Hyun An,[†] Seong Keun Kim,[‡] and Cheol Seong Hwang*,[†]

[†]Department of Materials Science and Engineering and Inter-University Semiconductor Research Center, Seoul National University, Seoul 151-742, Republic of Korea

[‡]Electronic Materials Research Center, Korea Institute of Science and Technology, Seoul 136-791, Republic of Korea

ABSTRACT: The effects of Al doping in atomic-layer-deposited HfO_2 (AHO) and ZrO_2 (AZO) films on the evolutions of their crystallographic phases, grain sizes, and electric properties, such as their dielectric constants and leakage current densities, were examined for their applications in high-voltage devices. The film thickness and Al-doping concentration were varied in the ranges of 60−75 nm and 0.5−9.7%, respectively, for AHO and 55−90 nm and 1.0−10.3%, respectively, for AZO. The top and bottom electrodes were sputtered Mo films. The detailed structural and electrical property variations were examined as functions of the Al concentration and film thickness. The AHO films showed a transition from the monoclinic phase (Al concentration up to 1.4%) to the tetragonal/cubic phase (Al concentration 2.0−3.5%), and finally, to the amorphous phase (Al concentration >4.7%), whereas the AZO films remained in the tetragonal/cubic phase up to the Al concentration of 6.4%. For both the AHO and AZO films, the monoclinic and amorphous phases had dielectric constants of 20−25, and the tetragonal/cubic phases had dielectric constants of 30−35. The highest electrical performance levels for the application to the high-voltage charge storage capacitors in flat panel displays were achieved with the 4.7−9.7% Al-doped AHO films and the 2.6% Al-doped AZO films.

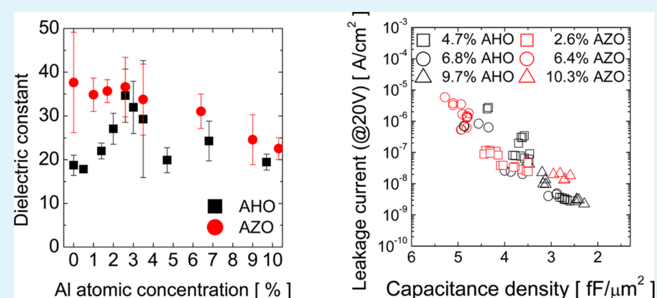

KEYWORDS: *atomic layer deposition, Al-doped HfO_2, Al-doped ZrO_2, leakage current, dielectric constant, phase evolution, grain size*

■ INTRODUCTION

Many high-dielectric-constant (κ) materials have been examined for capacitor application in diverse electronic devices that include the next-generation dynamic random access memory (DRAM),[1−3] multilayer ceramic capacitor (MLCC),[4] and charge storage capacitor in flat panel displays (FPDs).[5] While research on high-κ capacitors in DRAMs has been very active in past decades,[1] the application of high-κ capacitors as charge storage capacitors in FPDs is relatively new, and only a handful of studies on it could be found in literature. The high-κ capacitor materials for MLCC have been limited to (cation-doped) $BaTiO_3$ powders for a long time due to their historical background, but the thin-film-type MLCC recently started attracting greater interest.[6,7] However, the required electrical performance levels for each device application are very diverse due to the highly disparate operating conditions, such as the device voltage, clock speed, and allowed charge loss. The charge storage capacitor in FPDs has generally different specifications from the capacitors for DRAM. A high capacitance is required to ensure the color brightness of each pixel in the active-matrix-type organic light-emitting diode (AMOLED), but a similar level of importance is assigned to the low leakage current for the storage of sufficient charge during the off time of the OLED-driving thin film transistor. The voltage applied to the charge storage capacitor in FPDs is 15−20 V, which is more than 1 order of magnitude higher than that applied in DRAM. However, the needed capacitance density in FPD is several fF/μm^2, which is lower than that for DRAM by approximately 1 order of magnitude. Therefore, the HfO_2- and ZrO_2-based high-κ dielectrics, which have been extensively studied in the semiconductor industry for both logic transistors and memory, could be viable solutions to this application when their thickness is appropriately increased to several tens of nanometers from only several nanometers in semiconductor devices.

It is widely known that the κ value and energy band gap of dielectric materials are inversely correlated, which makes higher-κ titania dielectric materials such as rutile-structured TiO_2 ($\kappa \sim 100$ at a thickness of ~10 nm) and $SrTiO_3$ ($\kappa \sim 150$ at a thickness of ~10 nm) prevalently exhibit an exacerbated leakage current property due to their smaller band gap ($E_g \sim$ 3.0−3.2 eV) and generally low band offsets with metal electrodes.[8−10] HfO_2 and ZrO_2 have much higher E_g values (~5.5−6.0 eV) than titania materials. Such higher E_g values could generally result in a conduction band offset with a metal electrode, typically Mo in FPDs, of ~2 eV, which is higher than

Received: September 23, 2014
Accepted: November 25, 2014
Published: November 25, 2014

 © 2014 American Chemical Society dx.doi.org/10.1021/am506525s | ACS Appl. Mater. Interfaces 2014, 6, 22474−22482

that (~1 eV) between titania and a typical high-work-function metal, and these make the leakage-current-related risks much lower. The κ values of these materials are 15−20 when they are in the thermodynamically stable monoclinic phase (m-phase) at the typical thin film growth conditions [several Torrs of pressure and ~200−300 °C temperature for atomic layer deposition (ALD)]. Although these κ values are higher than those of low-κ materials such as SiO_2 (κ = 3.9), Si_3N_4 ($\kappa \sim 7$), and Al_2O_3 ($\kappa \sim 9$), they are not high enough for several applications, such as ultrahigh-definition FPDs. For example, when 15 V is applied to a SiO_2 film with a thickness of 10 nm, which corresponds to a capacitance density of 3.45 fF/μm^2 (useful for FPD application), the resulting electric field is 15 MV/cm, which is higher than the breakdown limit of thermal SiO_2. Thus, SiO_2 cannot be used in FPDs. When the κ value of a dielectric is 16, 41 nm of its thickness can result in the same capacitance density, but the electric field over this dielectric layer at the same 15 V is 3.7 MV/cm, which is comparable to the dielectric breakdown field of HfO_2. This suggests that HfO_2 or ZrO_2 with a κ value of <20 is also inappropriate as a dielectric material for FPDs.

There have been extensive studies to increase the κ values of HfO_2 and ZrO_2 materials by changing their phase to the metastable tetragonal phase (t-phase) or the cubic phase (c-phase), the κ values of which are higher than 30,[11−14] but their E_g values did not decrease. While these phases are the thermodynamically stable phases at much higher temperatures than the ALD temperature at the atmospheric pressure,[15] the transition of the m-phase to these metastable phases, and the accompanying increase in the κ values, have been consistently observed.[13,14] Although there are several methods of inducing such a phase transformation, such as cation doping,[16−18] carbon impurity incorporation,[19] production of oxygen-deficient phases,[20] and alloying of ZrO_2 and HfO_2,[21] the fundamental driving force for such a transition is a surface energy in higher-symmetry phases (cubic and tetragonal) lower than that in the lower-symmetry phase (monoclinic).[12] Therefore, growing thin film materials with smaller grain sizes, which would prefer the higher-κ-value phases, has been the main method of achieving such higher-κ phases in HfO_2 and ZrO_2. It was recently reported that this type of phase transition could be adopted to induce orthorhombic phases, which are stable at high pressures (3−5 GPa hydrostatic pressures) and even have ferroelectric properties.[22] This is a notable example of the substantial influence of the surface energy on the phase stability and accompanying properties of high-κ dielectric materials. It has been reported that the critical grain sizes (CGSs) for inducing such transition from the m-phase to the t- or c-phases are ~5−10 nm and ~25−30 nm for the HfO_2 and ZrO_2 films, respectively.[19,22−26] The clear identification of the t- and c-phases in thin films using the laboratory X-ray diffraction method is, however, generally difficult due to the severe overlap of the diffraction peaks in the two phases, as was the case in this study, so the higher-κ phases are generally termed the "t/c-phase." The smaller CGS of HfO_2 than that of ZrO_2 could be ascribed to the smaller difference between the surface energies in the m- and t/c-phases than that in ZrO_2.[22]

Thin oxide films generally start to grow in ALD with nucleation on the heterogeneous substrate surface and the nuclei coagulate to later form continuous films. Meanwhile, tiny (only several nanometers in diameter) nuclei with an amorphous structure generally start to form, which could be due to the much lower growth temperature (200−300 °C) than the melting point of such oxides (~2700 °C). However, sooner or later, they are transformed to the crystalline phase due to the accumulated excess bulk free energy of the amorphous material compared with the stable crystalline phases. This appears to occur at the cluster (nuclei) size of ~10 nm.[22] Thus, ZrO_2 tends to crystallize with the metastable t/c-phase structure even without doping because it is smaller than the CGS, and HfO_2 tends to crystallize with the stable m-phase structure due to its smaller CGS. Therefore, appropriate doping is needed to induce the transformation of the m-phase to the t/c-phase in the case of HfO_2,[16−18] but not necessarily in the case of ZrO_2.[27]

It has been theoretically estimated that the doping of HfO_2 and ZrO_2 with several cations, such as Si, Al, and Y, decreases the difference in the volume-free energies of the t/c-phase and the m-phase,[16] which eases the transformation from the m-phase to the t/c-phase with slightly larger grain sizes. When this aspect is considered in the examination of the crystallization of amorphous nuclei into the m-phase or the t/c-phase during the ALD of HfO_2 and ZrO_2 films, it can be understood that the doping can increase in the CGS, which will make the transformation to the t/c-phase feasible, even in the case of HfO_2. According to this idea, ALD cycles of Al_2O_3 were introduced during the HfO_2 and ZrO_2 ALD processes with controlled cycle ratios of Al−O to Hf−O and Al−O to Zr−O ALD processes to control the Al concentration in the film and to observe the phase transition. This is actually unnecessary in the case of ZrO_2 because ZrO_2 could grow with the t/c-phase structure without Al doping, as mentioned earlier. In fact, in this study, the incorporation of Al_2O_3 into ZrO_2 with a relatively high concentration degraded the κ value due to the lower κ value of the Al_2O_3 itself, which is an undesirable aspect of this approach. However, it is also known that the doping of a ZrO_2 thin film with Al ions generally decreases the leakage current and increases the breakdown field.[28] Therefore, there may be room to improve the overall dielectric performance levels of ZrO_2 films through appropriate dosing of Al, at which the capacitance decrease is minimized and the leakage current is substantially decreased.

In the case of HfO_2, however, doping the film with Al_2O_3 will induce two effects on the κ value. An increase in the Al concentration induces first an increase in the κ value through the transformation to the t/c-phase, but a too high Al concentration eventually decreases the κ value due to the low κ value of Al_2O_3. Therefore, a certain optimum Al concentration is expected at which the κ value peaks. The leakage current is also expected to decrease with the appropriate Al doping in the case of HfO_2.

According to these ideas, relatively thick (Al-doped) HfO_2 and ZrO_2 thin films with various Al concentrations were grown using the ALD method on a Mo substrate. Moreover, the detailed crystallographic and chemical structures, along with the accompanying electrical performance levels, were examined for their possible applications as charge storage capacitors for AMOLED or AM liquid crystal display devices.

■ EXPERIMENTAL SECTION

The Al-doped HfO_2 (AHO) and Al-doped ZrO_2 (AZO) films were deposited using a traveling-wave-type ALD reactor at a wafer temperature of 250 °C. $Hf[N(CH_3)(C_2H_5)]_4$ (TEMAH), $Zr[N(CH_3)(C_2H_5)]_4$ (TEMAZ), and $Al(CH_3)_3$ (TMA) were used as the Hf, Zr, and Al precursors, respectively, and O_3 with a concentration of 250 g/m^3 was used as the oxygen source. The TEMAH/TEMAZ pulse, purge, O_3 pulse, purge, TMA pulse, and purge time were 4.5, 5,

3, 3, 0.5, and 25 s, respectively. DC-sputtered Mo (200 nm)/SiO_2 (100 nm)/Si substrates were used as the bottom electrodes (BEs), and different Al−O to Hf−O (Zr−O) ALD cycle ratios were adopted for the growth of the variously doped AHO and AZO films. To improve the quality of the films, they were annealed at 580 °C for 30 s under an N_2 atmosphere using a rapid thermal annealing (RTA) system. 580 °C is a temperature which commercial glasses in display industry are sustainable up to. To measure the electrical properties, a metal−insulator−metal (MIM) capacitor was fabricated with a 50 nm thick electron-beam-evaporated Mo top electrode (TE) using a metal shadow mask (with a 300 μm hole diameter). The top electrode was annealed at 360 °C for 1 h under an N_2 atmosphere using a vertical tube furnace to eliminate the damage effect of the electron beam deposition process.

The film thickness was measured via spectroscopic ellipsometry (J. A. Woollam, ESM-300) and X-ray reflection (XRR, PANalytical, X'Pert Pro). Glancing-angle X-ray diffraction (GAXRD, PANalytical, X'Pert Pro; incidence angle, 0.5°) was used to examine the evolution of the crystallographic phases according to the film thickness, Al concentration, and RTA conditions. The chemical composition and possible change in the bonding characteristics with Al doping were analyzed using X-ray photoemission spectroscopy (XPS, Sigma Probe, Thermo VG). The impurity concentration in the films, including carbon, and the depth profile were examined by Auger electron spectroscopy (AES, PerkinElmer, PHI 660, PHI 670). The surface topography was estimated using atomic force microscopy (AFM, JEOL, JSPM 5200) and scanning electron microscopy (SEM, Hitachi, S-4800). The electrical performance was studied by measuring the capacitance−voltage ($C-V$) and the current density−voltage ($J-V$) using a Hewlett-Packard 4140D and 4194A, respectively. The AC excitation frequency for the $C-V$ measurement was 10 kHz, and the capacitance values were measured at the DC bias voltage of 0 V. The estimated dielectric loss factor was generally < ~1%, which confirms the accuracy of the capacitance estimation. During the electrical tests, the TE was biased and the BE was grounded.

■ RESULTS AND DISCUSSION

Figure 1a shows the variations in the thicknesses of the undoped HfO_2 and ZrO_2 films as functions of the ALD cycles. The slope and the x axis intercept of the graphs (lines) that best linearly fit the experiment data (the open symbols) show that the thickness growth rates of the HfO_2 and ZrO_2 films were 0.13 nm/cycle and 0.16 nm/cycle, respectively,[14,29] and that almost no incubation cycle (number of ALD cycles wherein films did not grow) was observed in both cases. These growth rates are slightly higher than those reported for the thinner film (<10 nm) growth using an identical growth process, which suggests that the thicker films generally had a higher growth rate, probably due to their enhanced crystallization on the Mo electrode.[30] Figure 1b shows the variations in the Al concentration ([Al]/[Al] + [Hf] and [Al]/[Al] + [Zr]) in the AHO and AZO films which were determined by XPS as a function of the Al cycle ratio (the number of Al_2O_3 cycles/the other ALD cycles). The estimated error limit for the data shown in Figure 1b is < ~5%, which is provided by the XPS tool manufacturer. Here, the total number of ALD cycles was 600, which made the films 65 nm thick. It could be understood that the Al concentration varied linearly with the Al cycle ratio up to the Al concentration of ~10% in both cases, wherein the Al incorporation in the ZrO_2 was slightly more efficient than that in the HfO_2, which could be understood from the slightly positive and negative y-axis intercepts of the best linearly fit graphs. The growth rate of the Al_2O_3 film was ~0.1 nm/cycle. Because the XPS analysis is very sensitive to the surface region than the bulk or inside of the film, AES was used to confirm the concentration variation along the thickness direction. Figure 1c,d showed the AES depth profiles of AHO (Al cycle ratio ~0.14) and AZO (Al cycle ratio ~0.2) films, respectively. Because there was no appropriate standard for AES spectrum calibration, the atomic concentrations in these figures must be taken only as the relative numbers. It could be understood that Al showed uniform distribution across the entire film thickness for both cases, suggesting that the Al and Hf and the Al and Zr were well intermixed during the ALD or RTA making the uniformly doped films. Therefore, the Al concentrations of the films which were acquired by XPS analyses represent the Al compositions in the bulk of the HfO_2 and ZrO_2 films. AES analysis also revealed that there were residual carbon impurities of which concentrations were ~3% and ~2% in AHO and AZO, respectively.

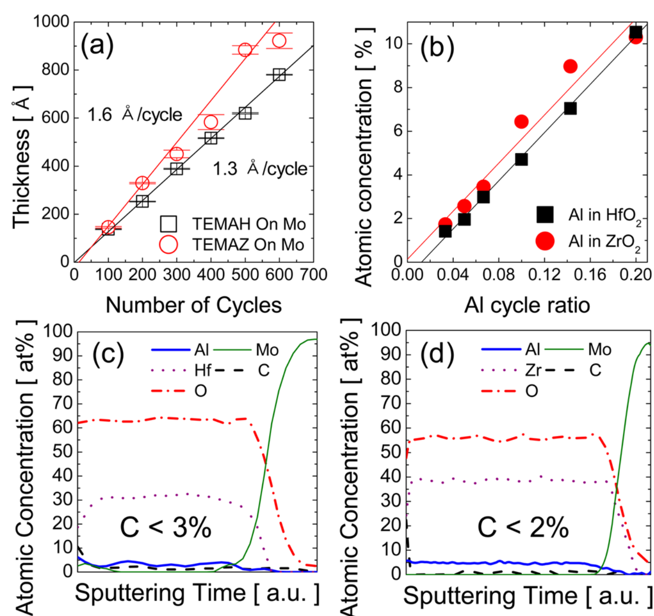

Figure 1. (a) Variations in the thicknesses of the undoped HfO_2 and ZrO_2 films as functions of the ALD cycles. (b) The variations in the Al concentrations ([Al]/[Al] + [Hf] and [Al]/[Al] + [Zr]) of the AHO and AZO films as functions of the Al cycle ratio (number of Al_2O_3 cycles/total number of ALD cycles). The AES depth profiles of (c) Al-doped HfO_2 (Al cycle ratio ~0.14, 90 cycles) and (d) Al-doped ZrO_2 (Al cycle ratio ~0.2, 120 cycles) films.

Figure 2 shows the collected XPS spectra of the Hf 4f, Al 2p and Zr 3d, Al 2p core levels in AHO and AZO, respectively, for the various Al concentrations. The peak position was calibrated with the adventitious carbon peak position (284.5 eV). Within

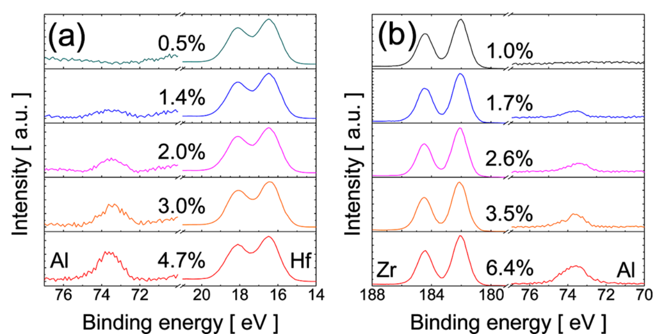

Figure 2. XPS core-level spectra of (a) Hf 4f, Al 2p and (b) Zr 3d, Al 2p for various Al concentrations.

the experiment error range (∼1%), there was no significant change in the peak shape and positions, which suggests that the Al doping hardly influenced the chemical environments of the Hf−O and Zr−O bindings, consistent with previous reports.[28,31] As the Al subcycle ratio increased, the intensity of Al core level spectra increased, but there was no discernible change in their binding energy and peak shape. However, the crystallographic structures of the films at the as-deposited state and after the annealing at 580 °C had substantial differences, as shown in Figures 3−6.

Figure 3 shows the GAXRD patterns of the as-deposited undoped HfO_2 and ZrO_2 films, respectively, with different film thicknesses. Even though the films were not postannealed, the 15 nm thick ZrO_2 film showed evident diffraction peaks, which revealed that the films were already crystallized, and the peak intensities increased with the increasing film thickness. The 11 nm thick HfO_2 film did not show notable diffraction peaks except for a strong peak near $2\theta \sim 41°$, which was Mo (110) peak. This suggests that the HfO_2 film has not yet crystallized. However, the thicker HfO_2 films evidently showed diffraction peaks from the oxide phases. While the HfO_2 films showed diffraction peaks mostly assigned to the m-phase, the ZrO_2 films showed peaks that corresponded to mostly the t/c-phases. The HfO_2 films also showed a weak diffraction peak near $2\theta \sim 36°$, which could be assigned to the t-phase (002) or the t-phase (110) planes, but its relative intensity actually dropped with the increasing film thickness. The ZrO_2 films also showed a tiny diffraction peak near $2\theta \sim 32°$, which might be assigned to the m-phase (111) plane, the intensity of which did not vary with the increasing film thickness. Another difference in the GAXRD patterns of the HfO_2 and ZrO_2 is that the ZrO_2 showed a higher relative peak intensity in the t-phase (011)/c-phase (111) when it was thin, but the relative intensity of the t-phase (002)/c-phase (002) peaks became dominant as the thickness increased, while the HfO_2 film showed no evident change in its relative peak intensity distribution. These GAXRD data suggest that the undoped HfO_2 and ZrO_2 films are predominantly crystallized into the m-phase and the t/c-phase, respectively, at their as-deposited state. Figure 4 shows the GAXRD patterns of the samples in Figure 3 after the RTA. They show that the RTA did not induce a notable difference in the GAXRD patterns from the as-deposited ones, except in the case of the 11 nm thick HfO_2 film, which crystallized to a mixture of the m-phase and the t-phase.

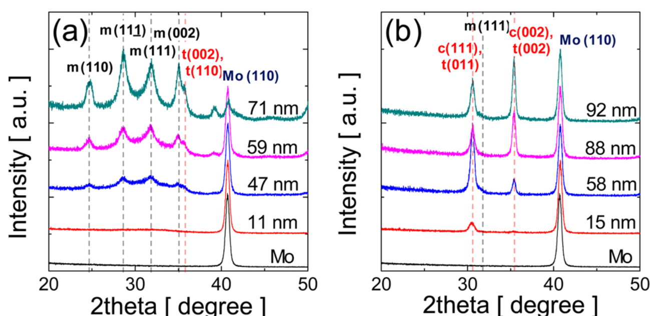

Figure 3. GAXRD patterns of the as-deposited (a) HfO_2 and (b) ZrO_2 films with different film thicknesses.

In contrast, the Al-doped films showed highly disparate GAXRD patterns for the HfO_2 and ZrO_2 films especially after the RTA. Figure 5 shows the GAXRD patterns of the as-deposited, 59−74 nm thick AHO and 69−88 nm thick AZO films with different Al concentrations. In the case of the AHO films, the increase in the Al concentration rapidly decreased the crystallization of the film, and the film with an Al concentration of only ∼2% showed no diffraction peak from the oxide layer. Moreover, all the AHO films with a higher Al concentration appeared to be amorphous. This means that the incorporation of Al atoms into the HfO_2 nuclei really suppressed the crystallization of the nuclei to the m-phase (and to other phases). In contrast, a clear diffraction peak from the crystallized ZrO_2 was observed up to the Al concentration of 6.4%, although the peaks generally shifted to the higher 2θ direction, which suggests a lower lattice constant due to the Al doping—perhaps a reasonable consequence of the smaller ionic radius of Al^{3+} (51 pm) than of Zr^{4+} (72 pm). Even with the Al doping, the crystalline phase was predominantly the t/c-phase. Therefore, the AZO was amorphorized by the Al doping only when the Al concentration was > ∼9%. An interesting finding is that the decreased rate of the t(002)/c(002) peak was faster than that of the t(011)/c(111) peak with the increasing Al concentration, which was also the case when the crystalline quality was degraded by the decreasing film thickness in the case of the undoped ZrO_2. This might be related to the anisotropy of the surface energies along the different crystallographic indices, which requires further study for more detailed understanding. Figure 6 shows the GAXRD patterns of the samples shown in Figure 5 after the RTA. While the AZO films did not show any notable variation in their diffraction peaks, except for a general increase in their intensities, the AHO films showed a substantial change in their diffraction pattern, which suggests a drastic change in their crystallographic structures after the RTA. First, when the Al concentration was lower than ∼1%, the films were still predominantly in the m-phase. However, when the Al concentration increased to 1.4%, the

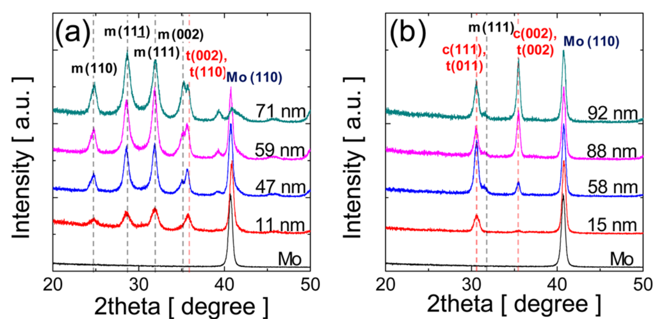

Figure 4. GAXRD patterns of the postannealed (a) HfO_2 and (b) ZrO_2 films with different film thicknesses. Postannealing was performed using the RTA process at 580 °C for 30 s under a N_2 atmosphere.

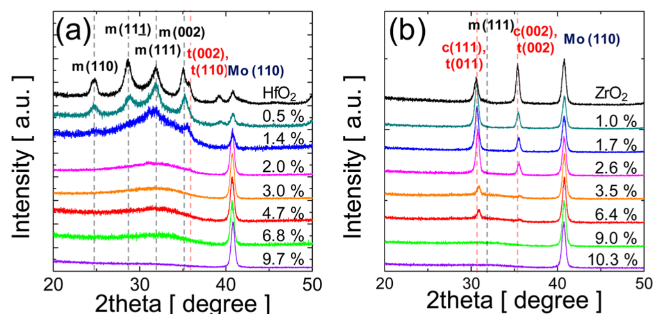

Figure 5. GAXRD patterns of the as-deposited (a) Al-doped HfO_2 and (b) Al-doped ZrO_2 films with different Al concentrations.

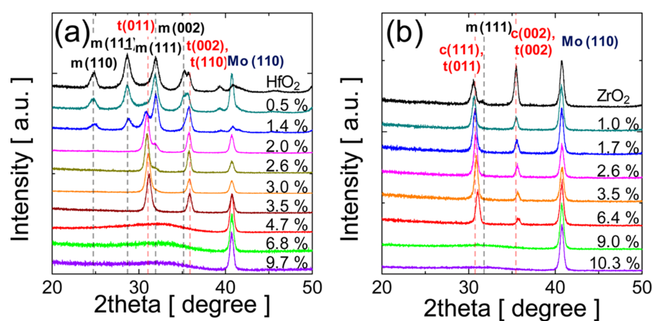

Figure 6. GAXRD patterns of the postannealed (a) Al-doped HfO_2 and (b) Al-doped ZrO_2 films with different Al concentrations. Postannealing was performed using the RTA process at 580 °C for 30 s under a N_2 atmosphere.

film was already predominantly in the t/c-phase, with a minor contribution from the m-phase. Up to the Al concentration of 3.5%, the films were almost completely in the t/c-phase, where the lattice parameter of the t/c-phase decreased with the increasing Al concentration, which could also be ascribed to the smaller ionic radius of Al^{3+} than of Hf^{4+} (78 pm). When the Al concentration was >4.7%, the AHO films were not crystallized even after the RTA. It is believed that such complicated crystallization behavior of the AHO must influence largely the dielectric properties (the κ value), which was indeed the case, as shown in the following section.

Before the electrical properties of the variously doped HfO_2 and ZrO_2 films were described, the variations in the surface morphologies with the variations in the Al concentration were examined via AFM and SEM. Figure 7 shows the AFM

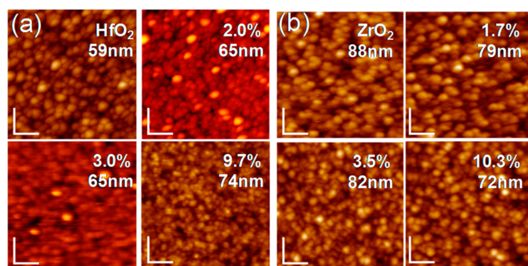

Figure 7. Selected AFM topographic images of the postannealed (a) Al-doped HfO_2 and (b) Al-doped ZrO_2 films with different Al concentrations (scale bar: 200 nm).

topographic images of the samples shown in Figure 6. For another comparison, the SEM images of the identical composition samples are shown in Figure 8, from which the average grain size could be estimated. The variations in the

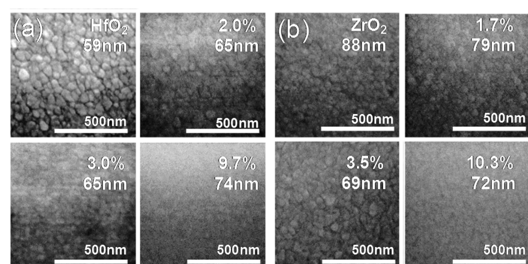

Figure 8. Selected SEM images of the postannealed (a) Al-doped HfO_2 and (b) Al-doped ZrO_2 films with different Al concentrations.

root-mean-squared (RMS) roughness value obtained from each AFM image as a function of the Al concentration are summarized in Figure 9a, and the corresponding variations in

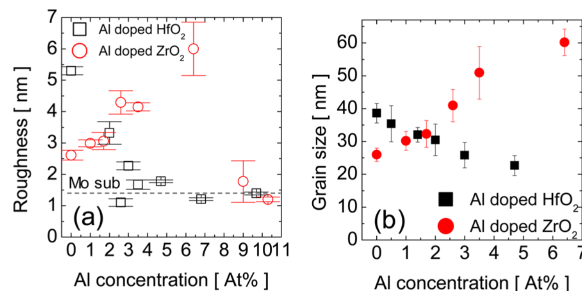

Figure 9. Summary of the variations in the (a) RMS roughness from the AFM images and (b) average grain size from the SEM images as a function of the Al concentration in the Al-doped HfO_2 and Al-doped ZrO_2 films.

the average grain size are summarized in Figure 9b. The variation in the RMS roughness of the AHO and AZO films showed an opposite trend with respect to the increasing Al concentration as long as the films were crystallized, and the roughness decreased and increased with the increasing Al concentration for the AHO and AZO up to the Al concentrations of ~5 and 7%, respectively. A further increase in the Al concentration yielded the amorphous films in both cases, which were reflected in the low RMS roughness (~1.5 nm) that was comparable to that of the Mo substrate (~1.3 nm). Such trends coincided well with the trends in the average grain size shown in Figure 9b. Because the AHO and AZO films with higher Al concentrations were amorphous, their grain size could not be estimated. Therefore, the changes in the crystallographic structures of the AHO and AZO films after the RTA could be explained well by the variation in the grain size with the increasing Al concentration. In the AHO films, the grain size decreased with the increasing Al concentration, so that they could be transformed from the m-phase when the Al concentration was low (which made the grain size large) to the t/c-phase when the Al concentration increased to up to ~4% (which made the grain size smaller). A further increase in the Al concentration made the film amorphous. In contrast, the AZO films showed a much smaller grain size than the AHO films when their Al concentration was low (< ~ 2%), but they showed a larger grain size at a higher Al concentration. Interestingly, the t/c-phase was retained in the case of the AZO, even at a grain size as large as ~60 nm, whereas in the case of the AHO, the 35−40 nm grain size was already too large to retain the t/c-phase. This may suggest that the apparently single-looking grains in the SEM of the AZO especially when the Al concentration was 5−7% were not really single grains but clusters of smaller real grains with slightly different crystallographic directions. This might be supported by the heavy distortion of the lattice at such a high Al concentration, which could be understood from the large peak shift in the high 2θ direction and the broadened peak shape in Figure 6b. Because the grain size estimation by SEM could reveal only the size in lateral dimension, the GAXRD data were analyzed using the Scherrer formula to complement the SEM results. In principle, applying the Scherrer formula to the XRD data can give a reasonable estimation to the grain size along the depth direction for the case of thin film provided that the divergence of the incident X-ray is small enough. While the glancing angle

diffraction geometry is not optimum for such purpose, and the XRD equipment in this work did not guarantee very small divergence angle, the grain size was estimated from the full-width half-maximum values of the GAXRD peaks. For AZO, due to the involvement of only t- and c-phases, the grain size analysis was rather straightforward, and the results are in qualitative agreement with the SEM; the vertical grain size slightly increases with the increasing Al concentration. However, the grain size estimated by SEM was ∼25−65 nm while grain size estimated in this way was ∼15−20 nm. This might be understandable as the XRD spectra were quite sensitive to the slight misorientation between the smaller grains that form the aggregates with similar crystallographic orientations (mosaic structure), which often seemed to be a single grain in SEM, while SEM was not. In contrast, the XRD results from the AHO were quite complicated, and no clear tendency could be found. While the SEM showed a general decrease in the grain size with the increasing Al concentration, no such tendency could be found from the GAXRD data, although the estimated grain sizes showed a wider coverage from ∼7 to ∼17 nm, which was quite dependent on the type of diffraction peaks. This might be understood from the involvement of the m-, t-, and c-phases, which made the evolution of grains into a certain phase very complicated. In fact, the degree of decrease in the grain size with the increasing Al concentration of AHO observed by SEM was smaller than that of the AZO reflecting the complicated evolution of the phases. The larger variation of the estimated grain sizes from different diffraction peaks also reflected such tendency.

The variations in the growth rates of the AHO and AZO films as a function of Al concentration are shown in Figure 10a.

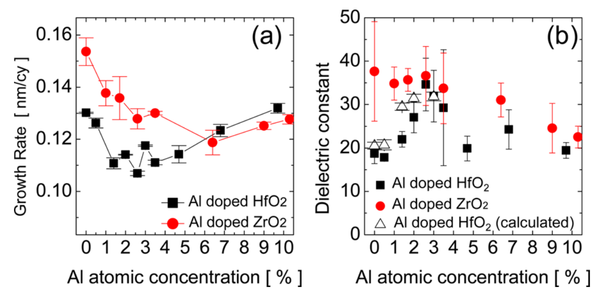

Figure 10. Variations in (a) growth rate and (b) the dielectric constant of the Al-doped HfO_2 and Al-doped ZrO_2 films as a function of the Al concentration. The dielectric constant of Al-doped HfO_2 and Al-doped ZrO_2 was obtained after the post deposition annealing. For the calculated dielectric constant, quantification of the constituent crystalline phases was performed using the GAXRD data, and dielectric constants of m- and t/c- phases were assumed to be 18 and 35, respectively.

These data were estimated by simply dividing the film thickness by number of total ALD cycles. For AZO, the growth rate showed a general decrease with the increasing Al concentration up to 6.4 atomic %, which corresponds to the t- and c-phase region. As the main constituent of the film growth process is still ZrO_2 deposition, this means that the ALD rate of ZrO_2 on Al−O covered surface was lower than that on its own. A similar effect has been reported for the case of Al-doped TiO_2 films, of which detailed mechanistic study can be found elsewhere.[32] This can be fundamentally ascribed to the stronger chemical bonding energy between Al and O compared with the Zr and O. When the growing film surface was covered with Al−O, the subsequently pulsed Zr-precursor molecules have less chance to be chemically adsorbed onto the Al−O surface compared with the Zr−O surface since the Al more strongly binds O than Zr. In the case of the O_3-based ALD, the surface of the film surface is covered with O*, which is the oxygen radical dissociated from O_3 molecules, immediately prior to the next metal precursor pulse.[33] Therefore, the stronger tendency to attract the surface oxygen to the underlying metal atoms would retard the active chemical reaction between the O* and incoming metal precursor, which is in this case TEMAZ. Nevertheless, such explanation may not be valid if the growing surface changes its crystallographic structure as for the cases with higher Al concentration (amorphous). In the amorphous case, the growth rate slightly increased with the increasing Al concentration, which cannot be explained by the aforementioned model. Such an effect has not been reported yet. However, more detailed discussions on this aspect are certainly over the scope of this work and would be a topic for future work. AHO films also showed similar trends; up to the Al-concentration of ∼2 atomic %, which corresponded to the crystalline region, the growth rate decreased quite rapidly, but slightly increased when it was higher than that concentration. Due to these variations in the growth rate with the varying Al concentrations, the precise control of the film thickness to a common value was rather difficult, although it was already attempted. However, the difference was not so large compared with the thicknesses themselves, and the different thickness effects could be mitigated by considering the electric field rather than voltage for the electrical tests.

Figure 10b shows the variations in the dielectric constants of the AHO and AZO films after the RTA, which were estimated from the capacitance densities of the samples shown in Figure 6. For the undoped HfO_2 and ZrO_2 samples, the κ values were ∼19 and 38, respectively, which correspond well with the reported values of the m-phase HfO_2 and the t/c-phase ZrO_2.[18,27] With the increasing Al concentration, the AZO films showed a monotonic downward trend in their κ values. Their κ values reached ∼23 when the Al concentration was 10.3%, which showed an amorphous structure. Such κ value is slightly too high for a completely amorphous material, so there must be nanocrystalline ZrO_2 t/c-phases embedded in the apparently amorphous AZO films. In contrast, the AHO showed an increasing trend in its κ value up to the Al concentration of 2.6%, which could be understood from the transition from the m-phase to the t/c-phase. At this Al concentration, the maximum κ value was ∼35, which was consistent with the κ value of the t/c-phase HfO_2.[12,13] With the further increase in the Al concentration, the κ value rapidly dropped to up to a 3.5% Al concentration but was still as high as 30 due to the retained t/c-phase structure. However, only at the 4.7% Al concentration, the film showed a highly degraded crystalline quality in its GAXRD pattern (Figure 6a), which is reflected in the significant decrease in the κ value to ∼20 in Figure 10. The films with even higher Al concentrations showed κ values of 20−25, which also suggested that there could have been nanocrystalline AHO grains that were too small to be detected by GAXRD or SEM. Up to the Al concentration of 4.7% in AHO films, the quantification of the constituent phases was attempted using the XRD data assuming that there was no amorphous phase involved as long as the diffraction peaks were observed. It was further assumed that the dielectric constants of m- and t-/c- phases are 18 and 35,[33−36] respectively, and the overall dielectric constant was calculated assuming the parallel

configurations of the two phases (black triangle symbol in Figure 10b). While these were rather crude assumptions, because there could be residual amorphous phase, and the two phases may not be in a parallel geometry, the comparison between the calculation and experimental data showed reasonable agreement. This strongly suggested that the main reason for the variation of the dielectric constant in AHO film was the variation in the crystalline phases according to the Al-doping.

However, it must be pointed out that the higher κ value among those of the various composition films did not necessarily correspond to the best electrical performance that showed the lowest and highest capacitance densities. This is because the higher capacitance density could be achieved when the dielectric film becomes thinner, although the κ value of the specific film did not peak when the leakage current was low enough. This could be well understood from the following explanation.

Figure 11 summarizes the representative current density−electric field (J−E) curves of the AHO and AZO films,

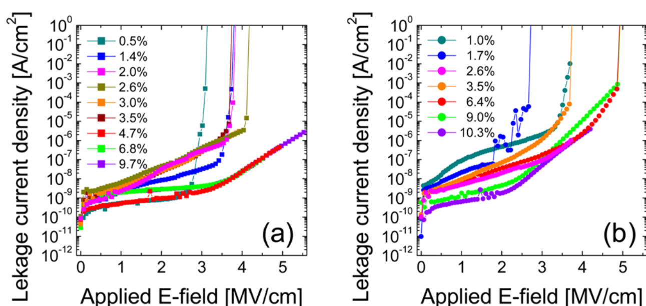

Figure 11. Summary of the representative current density−electric field curves of the (a) Al-doped HfO_2 and (b) Al-doped ZrO_2 films.

respectively. Here, the electric field was calculated by dividing the applied voltage by the film thickness, which might not be so accurate if the κ values are inhomogeneous across the film thickness[37] or if the film has a high space charge density.[38] The former problem was especially serious when the film was very thin (< ∼10 nm) due to the almost inevitably present various chemical and physical low-κ layers (dead-layer effect). However, the higher thickness range in this investigation (> ∼60 nm) mostly eliminates this concern. It is believed that the high-quality ALD films after the RTA did not have such a high defect density (not much higher than 10^{19} cm^{-3}). Therefore, the space charge effect could also be safely disregarded.[39] These considerations suggest that estimating the electric field by dividing the voltage by the film thickness is reasonable. Nevertheless, it is necessary to carefully consider the film thickness, dielectric constant, and leakage current density to compare fairly the performance of the various films with slightly different thicknesses as shown below.

Figure 11a shows a clear trend in the leakage current behavior of the AHO films according to their Al concentration. When the Al concentration was very low (< ∼ 1%), as in the m-phase, the films showed a very low breakdown field (∼3 MV/cm), which made them vulnerable to permanent electrical damage during the repeated voltage application in the devices, although their leakage current levels at fields below the breakdown field were very low ($<10^{-9}$A/cm^2). In the intermediate Al concentration range (1.4−3.5%), wherein the films were mostly in the t/c-phase, the breakdown field was increased to ∼3.5−4 MV/cm, but the leakage current in the electric field below the breakdown field was generally higher (10^{-9}−10^{-6}A/cm^2). When the Al concentration was higher than 4.7%, as in the amorphous phase, the leakage current significantly decreased, and no obvious breakdown was observed even at an electric field higher than 5.5 MV/cm, with the very low leakage current ($<10^{-9}$ A/cm^2) in the field of below 4 MV/cm, which is the typical field region for the operation of FPD devices. Therefore, amorphous films must have highly reliable leakage currents even though their κ values are slightly low.

The AZO films showed generally inferior leakage current properties than the AHO films, as can be understood from the J-E curves in Figure 11b. The curves show a consistently improving J-E trend with the increasing Al concentration, where the breakdown field increased and the leakage current in the field below the breakdown field decreased with the increasing Al concentration. This contradicts the topology data shown in Figure 9. It was generally anticipated that the greater roughness ascribed to the large grain size could induce a higher leakage current due to the local field concentration effect. However, with a significant film thickness (>60 nm), such effect appeared to have played no crucial role in the leakage current flow. In contrast, the number of grain boundaries, which might have acted as the high leakage current paths,[39] decreased with the increasing grain size per unit area, which may explain the decreasing current with the increasing Al concentration (larger grain size) of the AZO film. The amorphous AZO films (with an Al concentration >9.0%) showed the lowest leakage current, which could be ascribed to their lack of grain boundaries. However, the maximum breakdown field was still <5 MV/cm, which is obviously inferior to the breakdown property of amorphous AHO films even with a lower Al concentration. Therefore, it could be stated that the possibility of achieving better electrical performance must be higher in the case of the AHO than of the AZO, which could be confirmed in Figure 12.

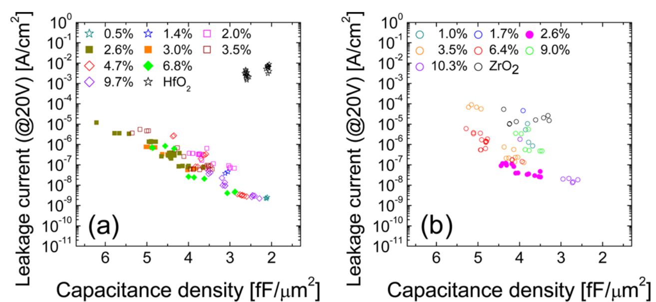

Figure 12. Summary of the electrical performance levels of the (a) Al-doped HfO_2 and (b) Al-doped ZrO_2 films, represented by the relationship between the leakage current density at 20 V and the capacitance density.

Figure 12 summarizes the overall electrical performance of the AHO and AZO films, respectively, as represented by the relationship between the leakage current density at a certain voltage (in this case, 20 V) and the capacitance density. Each dot in the figure coincides with a film with a certain Al concentration and thickness. The same color and shape symbol represent the same Al concentration but a different thickness. The estimated error limit for the data points shown in Figure 12 is ∼5%, which cannot be shown in the figure due to the

dx.doi.org/10.1021/am506525s | ACS Appl. Mater. Interfaces 2014, 6, 22474−22482

involvement of so many data points. In this type of plot, the data points near the origin represent a higher capacitance density and a lower leakage current, which are the desirable electrical performance levels. In the case of the AHO films, all the data points lie along a single line, except for the samples with HfO_2. These samples showed too high a leakage current at this voltage, which could be inferred from Figure 11a, so they showed highly degraded electrical performance levels that make them unusable in FPD applications. Among the other Al-doped samples, the films with higher Al concentrations (4.7, 6.8, and 9.7%, amorphous structures) showed the most desirable performance levels, although such levels did not significantly differ from those of the other samples with slightly lower Al concentrations (dominantly t/c-phases). This suggests that the decreasing film thickness could compensate well for the degraded κ values (20−25) of the amorphous samples compared with those of the t/c-phases (30−35) and that the generally superior leakage current performance of the amorphous films did not induce severe leakage problems even with their decreased thickness.

The leakage current−capacitance density performance was slightly more scattered in the case of the AZO than of the AHO, as shown in Figure 12b. When the film was undoped or when its Al concentration was very low (<1.7%), the leakage current was too high to allow the film to be used in the application, as was the case with the AHO. At the AZO Al concentration of 2.6%, the performance was comparable to the best result of the AHO, which was obtained from the 6.8% Al-doped AHO. However, with a further increase in the Al concentration, the leakage current decrease was not as evident as in the case of the AHO, but the loss in the κ value overcompensated for the leakage current gain. Therefore, the overall performance was generally degraded, as was most evident with the 9.0% Al doping. When the Al concentration was 10.3%, the capacitance density was comparable to that of the AHO film with an Al concentration of 9.7%, but the leakage current was higher by ∼1 order of magnitude. Similar trends were observed in both the AHO and AZO cases when the leakage current was 15 V, although the data are not shown. Such data suggest that AHO films generally perform better than AZO films do as high-performance capacitors for FPD applications.

CONCLUSION

In conclusion, AHO and AZO films with various Al concentrations were deposited using the ALD method on a SiO_2/Si substrate with a Mo film as the top and bottom electrodes. The films were typically 50−80 nm thick, which was needed to maintain their high insulation properties at applied voltages of 15−20 V, which are required in the device specifications for FPDs, such as AMOLED. The as-deposited AHO films remained in the m-phase when the Al concentration was < ∼2% and retained their amorphous structure when their Al concentration was >2.0%. In contrast, the as-deposited AZO films showed mostly t/c-phases up to the Al concentration of 6.4%, and showed a decreasing lattice parameter with the increasing Al concentration. Moreover, they became mostly amorphous at an even higher Al concentration. By performing RTA at 580 °C for 30 s in a N_2 atmosphere, the AHO films with the Al concentrations of 2.0−3.5% were transformed to the t/c-phase, the κ-values of which were as high as 30−35. The AHO films with Al concentrations lower and higher than this specific Al concentration range showed the m-phase and the amorphous phase, respectively, the κ value of which was 20−25. The leakage current performance generally improved with the increasing Al concentration, and the amorphous films did not show a hard breakdown up to an electric field as high as 5.5 MV/cm. In contrast, the AZO films showed t/c-phases up to the Al concentration of 6.4%, the κ value of which decreased from ∼38 to 30 with the increasing Al concentration, and the films with even higher Al concentrations showed an amorphous phase with a κ value of 20−25. However, the leakage current performance was generally inferior to that of the AHO, and even the amorphous films showed a hard breakdown at an electric field of ∼5 MV/cm. According to these electrical properties, the best electrical performance levels were achieved from the 4.7−9.7% AHO films and the 2.6% AZO films. This suggests that AHO films are more useful in the fabrication of FPD devices than AZO films because their allowable Al concentration range for the best electrical performance level is higher and thus allows larger process variations.

AUTHOR INFORMATION

Corresponding Author

*E-mail: cheolsh@snu.ac.kr. Tel: 82-2-880-7535.

Notes

The authors declare no competing financial interest.

ACKNOWLEDGMENTS

This work was supported by the National Research Foundation of Korea (NRF) grant funded by the Korea government (MSIP; No. NRF-2014R1A2A1A10052979).

REFERENCES

(1) Kim, S. K.; Lee, S. W.; Han, J. H.; Lee, B.; Han, S.; Hwang, C. S. Capacitors with an Equivalent Oxide Thickness of < 0.5 nm for Nanoscale Electronic Semiconductor Memory. *Adv. Funct. Mater.* **2010**, *20*, 2989−3003.

(2) Hwang, C. S. Atomic Layer Deposition for Microelectronic Applications. In *Atomic Layer Deposition of Nanostructured Materials*; Pinna, N., Knez, M., Eds.; Wiley-VCH Verlag GmbH & Co. KGaA: Weinheim, 2011; pp 159−192.

(3) Hwang, C. S., Ed. *Atomic Layer Deposition for Semiconductors*; Springer: New York, 2014.

(4) Hiroshi, K.; Youichi, M.; Hirokazu, C. Base-Metal Electrode-Multilayer Ceramic Capacitors: Past, Present, and Future Perspectives. *Jpn. J. Appl. Phys.* **2003**, *42*, 1.

(5) Geffroy, B.; le Roy, P.; Prat, C. Organic Light-Emitting Diode (OLED) Technology: Materials, Devices, and Display Technologies. *Polym. Int.* **2006**, *55*, 572−582.

(6) Kim, K. M.; Lee, S. Y.; Choi, G. J.; Han, J. H.; Hwang, C. S. Electrically Benign Dry-Etching Method for Rutile TiO_2 Thin-Film Capacitors with Ru Electrodes. *Electrochem. Solid-State Lett.* **2010**, *13*, G1−G4.

(7) Kambara, H.; Schneller, T.; Waser, R. In *Chemical Solution Deposition of Functional Oxide Thin Films*; Schneller, T.; Waser, R.; Kosec, M.; Payne, D., Eds.; Springer: Vienna, 2013; Chapter 22, pp 547−570.

(8) Robertson, J. Band Offsets of Wide-Band-Gap Oxides and Implications for Future Electronic Devices. *J. Vac. Sci. Technol., B: Microelectron. Nanometer Struct.−Process., Meas., Phenom.* **2000**, *18*, 1785−1791.

(9) Jeon, W.; Rha, S. H.; Lee, W.; Yoo, Y. W.; An, C. H.; Jung, K. H.; Kim, S. K.; Hwang, C. S. Controlling the Al-Doping Profile and Accompanying Electrical Properties of Rutile-Phased TiO_2 Thin Films. *ACS Appl. Mater. Interfaces* **2014**, *6*, 7910−7917.

(10) Lee, W.; Han, J. H.; Jeon, W.; Yoo, Y. W.; Lee, S. W.; Kim, S. K.; Ko, C.-H.; Lansalot-Matras, C.; Hwang, C. S. Atomic Layer Deposition

of $SrTiO_3$ Films with Cyclopentadienyl-Based Precursors for Metal−Insulator−Metal Capacitors. *Chem. Mater.* **2013**, *25*, 953−961.

(11) Zhao, X.; Vanderbilt, D. Phonons and Lattice Dielectric Properties of Zirconia. *Phys. Rev. B: Condens. Matter Mater. Phys.* **2002**, *65*, 075105.

(12) Zhao, X.; Vanderbilt, D. First-Principles Study of Structural, Vibrational, and Lattice Dielectric Properties of Hafnium Oxide. *Phys. Rev. B: Condens. Matter Mater. Phys.* **2002**, *65*, 233106.

(13) Jung, H.-S.; Jang, J. H.; Cho, D.-Y.; Jeon, S.-H.; Kim, H. K.; Lee, S. Y.; Hwang, C. S. The Effects of Postdeposition Annealing on the Crystallization and Electrical Characteristics of HfO_2 and ZrO_2 Gate Dielectrics. *Electrochem. Solid-State Lett.* **2011**, *14*, G17−G19.

(14) Lee, J. H.; Yu, I.-H.; Lee, S. Y.; Hwang, C. S. Phase Control of HfO_2-Based Dielectric Films for Higher-κ Materials. *J. Vac. Sci. Technol., B: Microelectron. Nanometer Struct.−Process., Meas., Phenom.* **2014**, *32*, 03D109.

(15) Stacy, D. W.; Wilder, D. R. The Yttria−Hafnia System. *J. Am. Ceram. Soc.* **1975**, *58*, 285−288.

(16) Lee, C.-K.; Cho, E.; Lee, H.-S.; Hwang, C. S.; Han, S. First-Principles Study on Doping and Phase Stability of HfO_2. *Phys. Rev. B: Condens. Matter Mater. Phys.* **2008**, *78*, 012102.

(17) Tomida, K.; Kita, K.; Toriumi, A. Dielectric Constant Enhancement due to Si Incorporation into HfO_2. *Appl. Phys. Lett.* **2006**, *89*, 142902.

(18) Park, P. K.; Kang, S.-W. Enhancement of Dielectric Constant in HfO_2 Thin Films by the Addition of Al_2O_3. *Appl. Phys. Lett.* **2006**, *89*, 192905.

(19) Cho, D.-Y.; Jung, H. S.; Yu, I.-H.; Yoon, J. H.; Kim, H. K.; Lee, S. Y.; Jeon, S. H.; Han, S.; Kim, J. H.; Park, T. J.; Park, B.-G.; Hwang, C. S. Stabilization of Tetragonal HfO_2 under Low Active Oxygen Source Environment in Atomic Layer Deposition. *Chem. Mater.* **2012**, *24*, 3534−3543.

(20) Jang, J. H.; Jung, H.-S.; Kim, J. H.; Lee, S. Y.; Hwang, C. S.; Kim, M. Investigation of Oxygen-Related Defects and the Electrical Properties of Atomic Layer Deposited HfO_2 Films using Electron Energy-Loss Spectroscopy. *J. Appl. Phys.* **2011**, *109*, 023718.

(21) Triyoso, D. H.; Hegde, R. I.; Schaeffer, J. K.; Roan, D.; Tobin, P. J.; Samavedam, S. B.; White, B. E.; Gregory, R.; Wang, X.-D. Impact of Zr Addition on Properties of Atomic Layer Deposited HfO_2. *Appl. Phys. Lett.* **2006**, *88*, 222901.

(22) Park, M. H.; Kim, H. J.; Kim, Y. J.; Moon, T.; Hwang, C. S. The Effects of Crystallographic Orientation and Strain of Thin $Hf_{0.5}Zr_{0.5}O_2$ Film on Its Ferroelectricity. *Appl. Phys. Lett.* **2014**, *104*, 072901.

(23) Garvie, R. C. The Occurrence of Metastable Tetragonal Zirconia as a Crystallite Size Effect. *J. Phys. Chem.* **1965**, *69*, 1238−1243.

(24) Garvie, R. C. Stabilization of the Tetragonal Structure in Zirconia Microcrystals. *J. Phys. Chem.* **1978**, *82*, 218−224.

(25) Pitcher, M. W.; Ushakov, S. V.; Navrotsky, A.; Woodfield, B. F.; Li, G.; Boerio-Goates, J.; Tissue, B. M. Energy Crossovers in Nanocrystalline Zirconia. *J. Am. Ceram. Soc.* **2005**, *88*, 160−167.

(26) Shandalov, M.; McIntyre, P. C. Size-Dependent Polymorphism in HfO_2 Nanotubes and Nanoscale Thin Films. *J. Appl. Phys.* **2009**, *106*, 084322.

(27) Kim, S. K.; Hwang, C. S. Atomic Layer Deposition of ZrO_2 Thin Films with High Dielectric Constant on TiN Substrates. *Electrochem. Solid-State Lett.* **2008**, *11*, G9−G11.

(28) Zhou, D.; Schroeder, U.; Xu, J.; Heitmann, J.; Jegert, G.; Weinreich, W.; Kerber, M.; Knebel, S.; Erben, E.; Mikolajick, T. Reliability of Al_2O_3-Doped ZrO_2 High-κ Dielectrics in Three-Dimensional Stacked Metal-Insulator-Metal Capacitors. *J. Appl. Phys.* **2010**, *108*, 124104.

(29) Park, M. H.; Kim, H. J.; Kim, Y. J.; Lee, W.; Kim, H. K.; Hwang, C. S. Effect of Forming Gas Annealing on the Ferroelectric Properties of $Hf_{0.5}Zr_{0.5}O_2$ Thin Films with and without Pt Electrodes. *Appl. Phys. Lett.* **2013**, *102*, 112914.

(30) Jõgi, I.; Kukli, K.; Ritala, M.; Leskelä, M.; Aarik, J.; Aidla, A.; Lu, J. Atomic Layer Deposition of High Capacitance Density Ta_2O_5−ZrO_2 Based Dielectrics for Metal−Insulator−Metal Structures. *Microelectron. Eng.* **2010**, *87*, 144−149.

(31) Park, T. J.; Kim, J. H.; Jang, J. H.; Lee, C.-K.; Na, K. D.; Lee, S. Y.; Jung, H.-S.; Kim, M.; Han, S.; Hwang, C. S. Reduction of Electrical Defects in Atomic Layer Deposited HfO_2 Films by Al Doping. *Chem. Mater.* **2010**, *22*, 4175−4184.

(32) Kim, S. K.; Choi, G. J.; Kim, J. H.; Hwang, C. S. Growth Behavior of Al-Doped TiO_2 Thin Films by Atomic Layer Deposition. *Chem. Mater.* **2008**, *20*, 3723−3727.

(33) Lee, S. Y.; Kim, H. K.; Lee, J. H.; Yu, I.-H.; Lee, J.-H.; Hwang, C. S. Effects of O_3 and H_2O as Oxygen Sources on the Atomic Layer Deposition of HfO_2 Gate Dielectrics at Different Deposition Temperatures. *J. Mater. Chem. C* **2014**, *2*, 2558.

(34) McNeill, D. W.; Bhattacharya, S.; Wadsworth, H.; Ruddell, F. H.; Mitchell, S. J. N.; Armstrong, B. M.; Gamble, H. S. Atomic Layer Deposition of Hafnium Oxide Dielectrics on Silicon and Germanium Substrates. *J. Mater. Sci.: Mater. Electron.* **2008**, *19*, 119−123.

(35) Mueller, S.; Mueller, J.; Singh, A.; Riedel, S.; Sundqvist, J.; Schroeder, U.; Mikolajick, T. Incipient Ferroelectricity in Al-Doped HfO_2 Thin Films. *Adv. Funct. Mater.* **2012**, *22*, 2412.

(36) Ceresoli, D.; Vanderbilt, D. Structural and Dielectric Properties of Amorphous ZrO_2 and HfO_2. *Phys. Rev. B* **2006**, *74*, 125108.

(37) Seo, M.; Rha, S. H.; Kim, S. K.; Han, J. H.; Lee, W.; Han, S.; Hwang, C. S. The Mechanism for the Suppression of Leakage Current in High Dielectric TiO_2 Thin Films by Adopting Ultra-Thin HfO_2 Films for Memory Application. *J. Appl. Phys.* **2011**, *110*, 024105.

(38) Shin, J. C.; Park, J.; Hwang, C. S.; Kim, H. J. Dielectric and Electrical Properties of Sputter Grown $(Ba,Sr)TiO_3$ Thin Films. *J. Appl. Phys.* **1999**, *86*, 506−513.

(39) Ikeda, H.; Goto, S.; Honda, K.; Sakashita, M.; Sakai, A.; Zaima, S.; Yasuda, Y. Structural and Electrical Characteristics of HfO_2 Films Fabricated by Pulsed Laser Deposition. *Jpn. J. Appl. Phys.* **2002**, *41*, 2476.